Applied Catalysis B: Environmental 338 (2023) 122989

Contents lists available at ScienceDirect

Applied Catalysis B: Environmental

journal homepage: www.elsevier.com/locate/apcatb

Behavior of nickel supported on calcium-enriched hydroxyapatite samples for CCU-methanation and ICCU-methanation processes

Zouhair Boukha, Alejandro Bermejo-López, Unai De-La-Torre, Juan R. González-Velasco *

Chemical Technologies for Environmental Sustainability Group, Department of Chemical Engineering, Faculty of Science and Technology, University of the Basque Country UPV/EHU, P.O. Box 644, E-48080 Bilbao, Spain

ARTICLE INFO

Keywords:
CO_2 methanation
CCU
ICCU
Ni catalyst
CaO sorbent
Calcium-enriched hydroxyapatite

ABSTRACT

The viability of Ni supported on Ca-enriched hydroxyapatite (HAP) samples has been investigated for the intensification of CCU-methanation and ICCU-methanation decarbonization processes. Even working with a surface density of added Ca three times larger than that required for a deposition of a theoretical monolayer, there is no apparent segregation of its resulting phases. Moreover, the progressive addition of Ca dramatically increases both the number and the strength of basic sites. Likewise, this markedly increases the Ni dispersion and the density of Ni lattice defects. The addition of 1–3 wt% Ca induces a dramatic improvement of the CCU-methanation activity and selectivity, when compared with the Ni/HAP sample. The optimal catalyst shows a good resistance under a long-term stability test at 375 °C for 90 h TOS. A compromise between the surface basicity and the distribution of Ni active sites proves to be the key factor influencing the efficiency of the investigated materials. In the ICCU-methanation process the Ni/Ca(3)/HAP DFM with added Ca loading close to the theoretical monolayer exhibits the best performance. For instance, it proves to be the most efficient to convert the adsorbed CO_2 to CH_4, during the hydrogenation period, reaching a CH_4 density close to 155 μmol_{CH4} g^{-1} at 400 °C. It is supposed that the methanation activity involves CO_2 stored only on surface CaO species and it is most likely improved over DFMs exhibiting short Ni-CaO distances. Interestingly, the performance of our Ni/Ca(3)/HAP DFM clearly outperforms that reported over 15%Ni/15%CaO/Al_2O_3 and 9.3%Ni/CaO reference DFMs. We conclude that a dispersion on HAP support of Ca loadings close to the theoretical monolayer becomes a promising alternative to basic DFMs.

1. Introduction

The extreme global surface temperatures measured in the last decade evidence that our planet continues to warm. Actually, there is an increasing awareness that this is only the beginning of profound environmental changes posing severe risks for ecosystems [1,2]. According to many reports, this is mainly caused by human activities (e.g. combustion of fossil fuels for essential applications) that emit undesirable greenhouse gases (GHGs) [1–5]. This scenario becomes even more alarming considering the continuous global energy demand growth and the slow progress on the fight against global warming; since this is not really a matter of a high priority on the international political agenda.

It is known that carbon dioxide presents relatively high activity in trapping solar radiation and, among all GHGs, it is the most abundant in the atmosphere. Therefore, implementing strategies with regard to the re-utilisation of emitted CO_2 has become essential to reduce its current global concentrations to acceptable levels [2–8]. In this sense, the use of green hydrogen to convert CO_2 to synthetic natural gas (SNG) is considered one of the most attractive strategies to overcome this challenging issue [6–8]. Furthermore, from an economic point of view, the available facilities for SNG storage and transport would justify the viability of this strategy to bring substantial economic returns. Among different routes proposed in the literature, CO_2 Capture and Utilization for methanation (CCU-methanation) and Integrated CO_2 Capture and Utilization for methanation (ICCU-methanation) represent promising strategies for atmospheric CO_2 reduction [9–12]. The former (CCU--methanation) is an appropriate technology for free, abundant and non-toxic carbon source. However, CO_2 from complex mixtures requires an unavoidable purification process, which significantly increases the CO_2-supply cost. The ICCU-methanation operation, by contrast, offers the possibility of recycling (in-situ) the combustion waste gas as well as the re-utilization of residual heat generated. This process alternates a

* Corresponding author.
E-mail address: juanra.gonzalezvelasco@ehu.es (J.R. González-Velasco).

https://doi.org/10.1016/j.apcatb.2023.122989
Received 14 March 2023; Received in revised form 8 June 2023; Accepted 10 June 2023
Available online 19 June 2023

period of CO_2 adsorption and a subsequent period of methanation with hydrogen, where the use of a dual function material (DFM) appears to be necessary [12]. The latter generally contain a high surface area catalyst support, an adsorbent presenting a suitable distribution of basic sites and an active hydrogenation transition metal. Moreover, they should be tolerant to poisonous impurities present in realistic mixtures (e.g. SO_2) [13]. Owing to their high capacity to store CO_2 from complex mixtures the use of DFM materials allows working with a reduced energy input, necessary for CO_2 purification process, as well as reducing the transportation costs.

The development of active and resistant catalysts for the CO_2 methanation (Sabatier reaction) is still one of the remaining challenges for an effective application of the process. Though many studies, dealing with a number of transition metals, are presently available, Ru- and Ni-based catalysts are actually the most investigated [5–8]. Specially, Ni catalyst formulations have attracted a special attention because of their lower cost and high selectivity. However, despite their promising performance, there is still a large room for improvement concerning their overall activity and their resistance against deactivation. To address this issue, current research is essentially focused on the development of formulations with catalyst supports presenting suitable metal-support interactions [8]. Furthermore, since the activation of CO_2 is mainly favoured on the basic sites, their surface modification by incorporation of highly basic materials appears to be essential for a high catalytic performance [8]. In this sense, a wide series of basic oxides have been investigated as chemical promoters, e.g. CaO, MgO, K_2CO_3, Na_2CO_3, CeO_2 and La_2O_3 [2–5,14–21]. These studies have mainly been devoted to the analysis of the impact of promoter addition on the nature of the resulting surface basicity as well as the distribution of active Ni species. For instance, Yang et al. [19] studied the effect of CaO addition (10–30 wt%) on the performance of Ni/CaO-Al_2O_3 catalysts in the CO_2 methanation reaction. They found that CaO was beneficial for the catalytic activity due to its capacity to generate additional basic sites with high thermal stability. Interestingly, the best performance was observed over the catalyst presenting a CaO loading close to 20 wt%. The superiority of the latter was associated with the presence of well dispersed CaO species that hinder the incorporation of Ni into the Al_2O_3 lattice. In their study on the impact of CaO promoter on the speciation of the Ni active phase, Everett et al. [20] designed a Ca-modified Ni/ZrO_2 catalyst for CO_2 methanation. They observed that the presence of Ca markedly improved the catalytic performance, owing to the occurrence of coordinatively unsaturated site pairs composed of Ni^{2+} and Ca^{2+} species. These sites were suggested to be highly active for the C-O bond dissociation.

In recent years, the use of hydroxyapatite (HAP) materials as catalyst supports is receiving increasing attention in the literature [8,22–28]. In fact, a number of demanding reactions have been successfully assayed on them. Due to its unique properties such as thermal stability, ion-exchange ability, very limited water solubility and tunable surface chemistry this emerging class of materials is generally regarded as a promising alternative to the traditional supports. For instance, in our recent study on the activity of a Ni/HAP free-promoter in the CO_2 methanation reaction, we found that it clearly outperformed other Ni/Al_2O_3 and Ni/Na-zeolite reference materials [8]. Moreover, the modification with lanthanum significantly enhanced its activity and stability. Besides the influence of La addition on the number and thermal stability of the basic sites, the observed improvement was also associated with a positive effect on the dispersion of Ni species, their reducibility and the occurrence of a large density of highly active defects on Ni-La_2O_3 interface. However, the studied formulation (Ni/La/HAP) did not seem suitable for the ICCU-methanation process, since over the optimal DFM, the density of produced methane did not exceed 85 $\mu mol_{CH4}\ g^{-1}$ at 520 °C.

In the present study we investigate the effect of the surface calcium-enrichment on the performance of a Ni/HAP catalyst in the CO_2 methanation reaction, when operating under CCU-methanation and ICCU-methanation conditions. The choice of Ca as a surface modifier agent was made owing to its known ability to generate a synergistic effect with the HAP support and its high theoretical capacity to adsorb CO_2 (17.8 $mmol_{CO2}\ g^{-1}_{CaO}$) [29,30]. Moreover, regarding economic considerations, calcium is one of the most cost-effective chemical promoters. For Ca addition the corresponding salt has been added through impregnation of a stoichiometric HAP instead of the co-precipitation method. We have opted for this strategy in order to avoid a possible formation of undesirable/inactive Ca species such as tricalcium phosphate (TCP, $Ca_3(PO_4)_2$) and calcium pyrophosphate (β-CPP, β-$Ca_2P_2O_7$) phases [29]. It is expected that a simple impregnation of Ca can mainly allow the formation of surface CaO and/or $Ca(OH)_2$ species. The properties of Ni/Ca(x)/HAP catalysts have been studied by using complementary techniques, i.e. BET, XRD, H_2-TPR, CO_2-TPD, TPSR, TEM and XPS spectroscopy. With reference to the unmodified sample, the improved catalytic properties of the calcium-enriched samples have been linked to suitable surface chemistry as well as the distribution of the Ni species.

2. Experimental

2.1. Preparation of the catalysts

The HAP material presenting a stoichiometric composition was synthesized through the co-precipitation method, by mixing $Ca(NO_3)_2{\cdot}4\ H_2O$ and $(NH_4)_2HPO_4$ salt solutions (1 and 0.6 mol L^{-1}, respectively). Thereafter, ammonium hydroxide (NH_4OH) was added to adjust the pH of the suspension to 10. The latter was vigorously stirred at 80 °C for 16 h. The precipitate was recovered by filtration, washed and then dried at 120 °C overnight. The obtained HAP support was finally calcined for 4 h at 500 °C (5 °C min^{-1}).

The catalysts consisting of HAP modified with Ca and Ni, subsequently, were prepared by impregnation. The Ca-doped HAP samples were first prepared, using $Ca(NO_3)_2{\cdot}4\ H_2O$ solutions, presenting different added Ca contents (x = 1, 2, 3 and 4 wt%). After drying (120 °C, 12 h), they were calcined at 500 °C (5 °C min^{-1}) for 4 h. Thereafter, the Ni/Ca(x)/HAP catalysts were prepared by impregnation of as-synthesized HAP and four Ca-modified HAP samples, from aqueous solutions containing $Ni(OCOCH_3)_2{\cdot}4\ H_2O$ salt to obtain Ni content of 3.3 wt%. The resulting Ni/Ca(x)/HAP samples were dried (120 °C, 12 h) and finally calcined at 500 °C (5 °C min^{-1}) for 4 h. For their activation the catalysts were submitted to reduction in a 20% H_2/He flow at 500 °C (10 °C min^{-1}) for 1 h.

2.2. Characterization techniques

The experimental procedures for the surface area measurement according to Brunauer-Emmett-Teller (BET) method, wavelength dispersive X-ray fluorescence (WDXRF), X-ray diffraction (XRD), transmission electron microscopy (TEM), high-angle annular dark field (HAADF), X-ray photoelectron spectroscopy (XPS), temperature programmed reduction (TPR), temperature programmed desorption of CO_2 (CO_2-TPD) and temperature programmed surface reaction (TPSR) are detailed in Supplementary Material.

2.3. Catalytic activity experiments

2.3.1. Catalytic CCU-methanation process experiments

The catalytic CO_2 methanation reaction experiments were carried out at atmospheric pressure, using a continuous flow reactor. Prior to the reaction, the catalysts (250 mg, 160–250 μm) diluted with quartz, to reach a bed volume of 1.5 cm^3, were first pre-treated at 500 °C in a 20% H_2/He flow for 1 h and then cooled to 200 °C in He (100 $cm^3\ min^{-1}$). Thereafter, they were submitted to the reaction mixture (16% CO_2, 64% H_2 and 20% He), with a total flow of 125 $cm^3\ min^{-1}$ (WHSV = 30,000 $cm^3\ g^{-1}\ h^{-1}$), and reaction temperatures ranging between 200

and 500 °C.

Analyses of the effluent gases were performed using a gas chromatograph (490 Micro GC - Agilent Technologies). The CO_2 conversion (X_{CO_2}) and selectivity to CH_4 (S_{CH_4}) and CO (S_{CO}), respectively, were calculated as follows:

$$X_{CO_2} = \frac{F^{in}_{CO_2} - F^{out}_{CO_2}}{F^{in}_{CO_2}} \times 100 \quad (1)$$

$$S_{CH_4} = \frac{F^{out}_{CH_4}}{F^{in}_{CO_2} - F^{out}_{CO_2}} \times 100 \quad (2)$$

$$S_{CO} = \frac{F^{out}_{CO}}{F^{in}_{CO_2} - F^{out}_{CO_2}} \times 100 \quad (3)$$

where F^{in}_i and F^{out}_i represent the reactor input and output flow rates, respectively, of the molecule "i".

2.3.2. Catalytic ICCU-methanation process experiments

The prepared samples were also investigated as DFMs for ICCU-methanation process. For this, we evaluated their performance in typical CO_2 storage/methanation cycle conditions [8]. The samples (1 g, 300–500 μm) were first reduced in 20% H_2/Ar at 500 °C for 1 h. Thereafter, a series of CO_2 storage/methanation cycles were performed in temperatures ranging between 280 and 520 °C. The total inlet flow was equal to 1200 $cm^3\ min^{-1}$ (WHSV = 72,000 $cm^3\ g^{-1}\ h^{-1}$) and each cycle was composed of the following four consecutive steps:

(i) CO_2 adsorption in a 10% CO_2/Ar flow (1 min),
(ii) Ar purge (2 min),
(iii) hydrogenation with a 10% H_2/Ar flow (2 min), and
(iv) Ar purge for 1 min

The gas mixture composition (CO_2, CH_4, CO and H_2O) was determined using an on-line FTIR analyzer (MG 2030). The calibration was performed for a large number of infrared-active gases by using known concentrations for each gas. With the help of MG2000 software, the preloaded calibration data allows continuous measurement and recording of sample streams. The density of stored CO_2 and produced CH_4 and CO were estimated as follows:

$$Y_{CO2}(\mu mol\ g^{-1}) = \frac{1}{W}\int_0^t [F^{in}_{CO_2}(t) - F^{out}_{CO_2}(t)]dt \quad (4)$$

$$Y_{CH_4}(\mu mol\ g^{-1}) = \frac{1}{W}\int_0^t F^{out}_{CH_4}(t)dt \quad (5)$$

$$Y_{CO}(\mu molg^{-1}) = \frac{1}{W}\int_0^t F^{out}_{CO}(t)dt \quad (6)$$

where W represents the DFM weight.

3. Results and discussion

3.1. Properties of the activated catalysts

3.1.1. N_2 physisorption studies

The results corresponding to N_2 physisorption isotherms and the pore sizes distribution for the reduced Ni/Ca(x)/HAP catalysts are presented as Supplementary Material (Figs. S1 and S2, respectively). The resulting isotherms exhibit a very similar shape, all of them corresponding to mesoporous materials (Fig. S1). Moreover, according to Fig. S2, their pore size distributions present a maximum centered between 23 and 38 nm. Table 1 lists the textural properties of the catalysts, extracted from their isotherms analysis. With reference to the bare support (55 $m^2\ g^{-1}$), the impregnation of 3.2 wt% Ni does not affect significantly the main textural properties. However, the progressive addition of calcium provokes a systematic loss in the specific surface area, e.g. the measured S_{BET} for the sample with the highest Ca loading (Ni/Ca(4)/HAP) does not exceed 19 $m^2\ g^{-1}$, which is 2.8 times lower than that of the monometallic sample. The dramatic loss of the specific surface area of the Ni/Ca(4)/HAP sample can be linked to the pore blockage resulting from the largest added Ca amounts. In parallel, on this Ca-rich sample, the pore distribution maximum, Fig. S2, is significantly shifted to the lowest value (22 nm), compared with that observed on the rest of the investigated samples (38 nm). This suggests that at high loadings (> 3 wt%) the impregnated Ca species preferentially fill the largest pores of the support.

3.1.2. Structural properties

The reduced Ni/Ca(x)/HAP samples were also characterized by XRD, resulting in diffractograms reported in Fig. 1. The patterns of the bare support (HAP) reveal the formation of a unique phase, characteristic of the apatite structure presenting the space group $P6_3/m$ (JCPDS: 01–082–256). Furthermore, the positions of its characteristic peaks are not affected by the addition of either Ni and/or Ca. Interestingly, the diffractograms of all reduced Ni catalysts evidence a complete reduction of its species into metallic Ni sites (JCPDS: 89–7120). The estimation of the mean Ni particle sizes, using the Ni° peak broadness (Fig. 1b), shows that they are ranging between 10.4 and 20 nm (Table 1). However, no diffraction peak due to the surface Ca species (CaO, $Ca(OH)_2$ or $CaCO_3$) can be observed. This result points out that the Ca species are mainly highly dispersed on the HAP surface.

3.1.3. Morphology, distribution and particle size of surface species

Fig. 2 includes TEM images of Ni/Ca(x)/HAP catalysts, reduced at 500 °C. All analyzed samples exhibit Ni particles with a quasi-spherical shape. Table 1 summarizes the estimated average Ni particle size and dispersion. The monometallic sample (Ni/HAP) shows the largest average NP size (13.9 nm) followed by Ni/Ca(1)/HAP (13.8 nm). Likewise, according to Fig. 3a, both catalysts present the widest size distribution. However, further addition of calcium (2–4 wt%) results in a narrower distribution and a significant decrease in the Ni average particle size, indicating a positive effect of added Ca on the dispersion of supported Ni species. A similar behavior was previously reported in a study on Ni/Ca/Al_2O_3 catalysts [31]. The promoting effect of Ca on the

Table 1
WDXRF, BET, XRD and TEM data for the reduced Ni/Ca(x)/HAP samples.

Sample	WDXRF		BET			XRD	TEM		
	Ca/P	Ni, %	S_{BET}, $m^2\ g^{-1}$	V_p, $cm^3\ g^{-1}$	d_p, nm	d_{XRD}, nm	d_{TEM}, nm	D, %	S_{Ni}, $m^2\ g^{-1}$
HAP	1.66	0	55	0.41	27.7	-	-	-	-
Ni/HAP	1.65	3.3	53	0.37	26.0	15.9	13.9	8.9	1.41
Ni/Ca(1)/HAP	1.76	3.2	51	0.37	26.7	10.4	13.8	9.0	1.43
Ni/Ca(2)/HAP	1.79	3.3	49	0.35	25.6	13.4	9.4	13.2	2.09
Ni/Ca(3)/HAP	1.85	3.2	42	0.30	26.8	17.3	7.4	16.8	2.66
Ni/Ca(4)/HAP	1.88	3.4	19	0.12 s	20.3	20	6.1	20.4	3.24

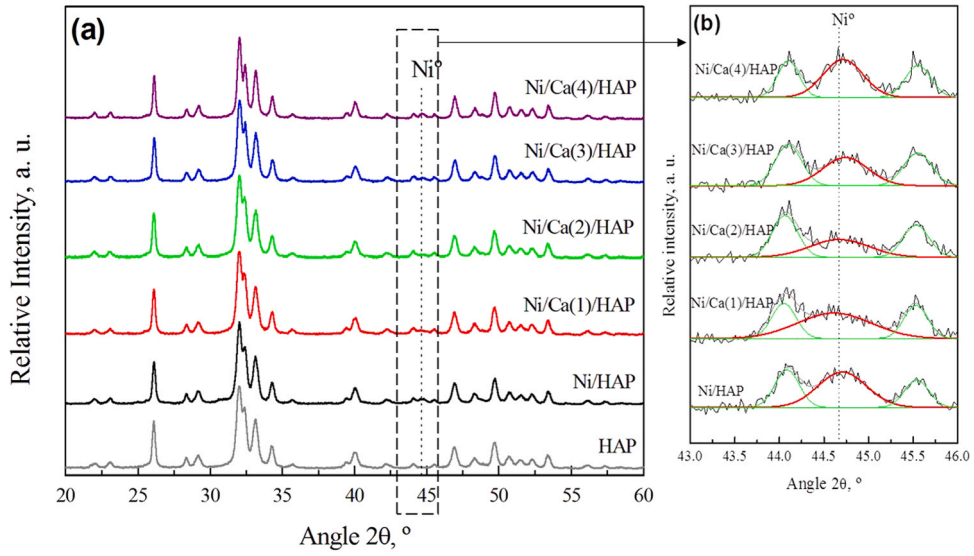

Fig. 1. (a) XRD patterns for the reduced Ni/Ca(x)/HAP samples and (b) zoom in the 2θ angle range of 43–46 °.

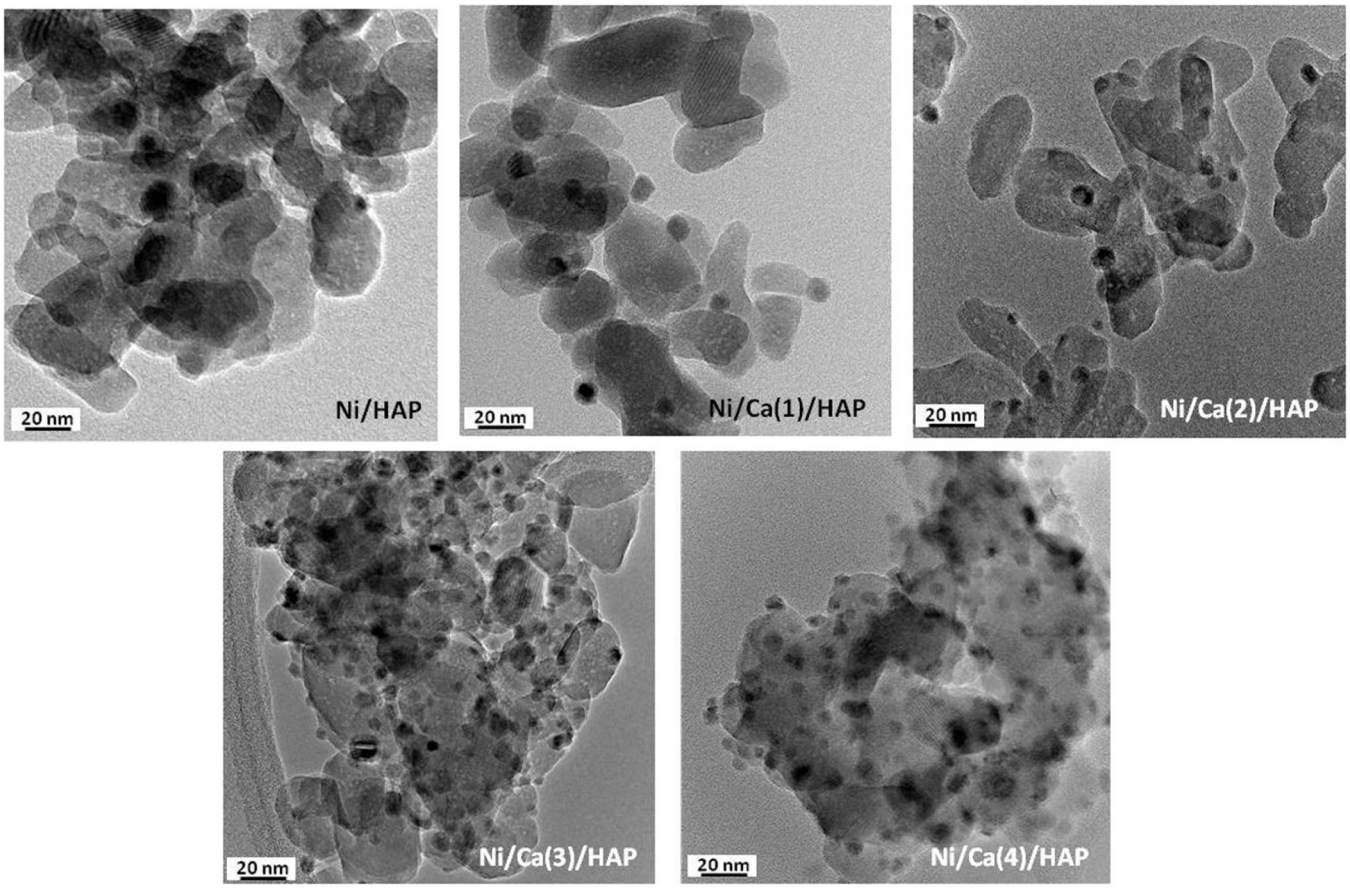

Fig. 2. TEM images for the reduced Ni/Ca(x)/HAP samples.

dispersion of Ni species was associated with the occurrence of a synergistic effect between Ni and Ca phases. It should be highlighted that this general trend contrasts that given by XRD analysis. Fig. 3b displays the dependence of the estimated degree of inconsistency (χ_i), between XRD and TEM data, on Ca loading. According to previous reports, the observed trend suggests an increase in the density of Ni crystallite imperfections with the progressive addition of Ca, which in turn implies an increase in the strength of metal-support interactions [8,32,33].

To gain further insight into the distribution of Ca species lying on the catalyst surface HAADF studies have been carried out on the Ni/Ca(2)/HAP and Ni/Ca(4)/HAP samples. Fig. S3 (a-f) show the HAADF images and the Ca and Ni maps for the two Ca-promoted samples. In accordance with the XRD data, the Ca maps for the two samples reveal that calcium is homogeneously dispersed, since no sparkling particles attesting a tridimensional growth of Ca species particles can be observed. This is actually a remarkable observation pointing out that, even working with

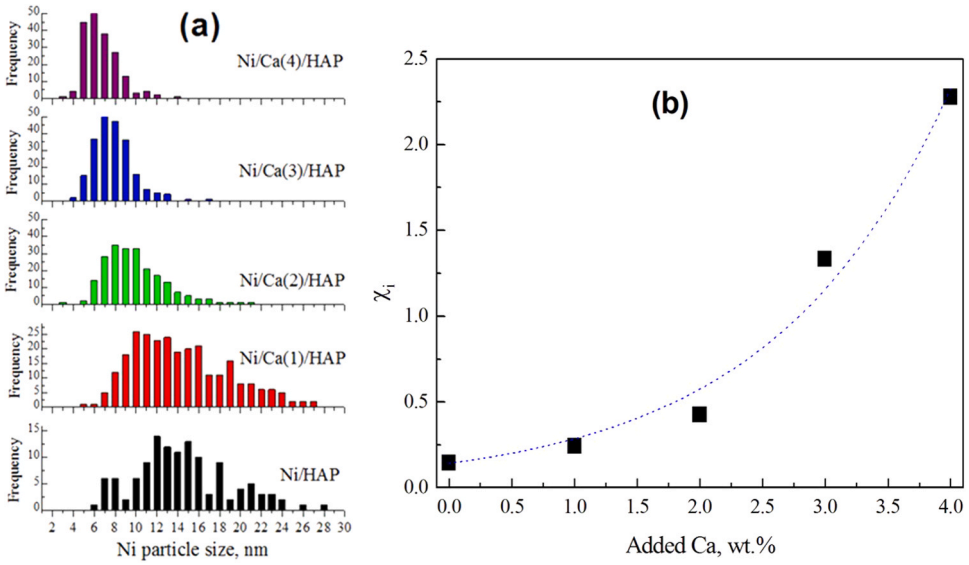

Fig. 3. (a) Histograms corresponding to the Ni particle sizes distribution. (b) Dependence of degree of inconsistency (χ_i), between XRD and TEM data, on added Ca loading.

a surface density of added Ca (31.6 Ca^{2+} nm^{-2} for Ni/Ca(4)/HAP), three times larger than that corresponding to a theoretical monolayer (10.3 Ca^{2+} nm^{-2}), there is no apparent segregation of its phases. In agreement with our previous study, this behavior suggests that the Ca surface enrichment pathway rather consists of a sequential deposition forming a thick layer [8,25].

3.1.4. *XPS analyses of the catalyst surface*

XPS analyses have been performed on the samples reduced in-situ to identify the chemical state of the elements lying on the catalyst surface. The main results of these studies are reported in Fig. 4, Fig. 5 and Table 2.

Fig. 4 shows that, in the Ni $2p_{3/2}$ region, all spectra consist of a main peak located at 852.5 ± 0.3 eV, accompanied by a shake-up satellite peak located between 857 and 858.5 eV. In good agreement with XRD data, these positions evidence the presence of metallic Ni as a unique phase [8,15,34]. Interestingly, with reference to the Ni/HAP sample (852.8 eV), the Ca-promoted samples exhibit lower BEs (852.2 ± 0.1 eV), suggesting the occurrence of Ni-Ca interactions affecting the electronic properties of supported Ni [34]. In parallel, data from Table 2 reveal a systematic increase of Ni/P atomic ratio with the progressive addition of Ca. In line with the TEM results, this tendency suggests that Ca addition improves the dispersion of Ni particles. Besides, according to Ca 2p spectra displayed in Fig. 5a, the Ni/HAP sample exhibits a typical Ca $2p_{3/2}$ peak, centered at 346.7 eV, assigned to Ca^{2+} ions in apatite materials [35,36]. Expectedly, Ca addition induces subtle changes in the

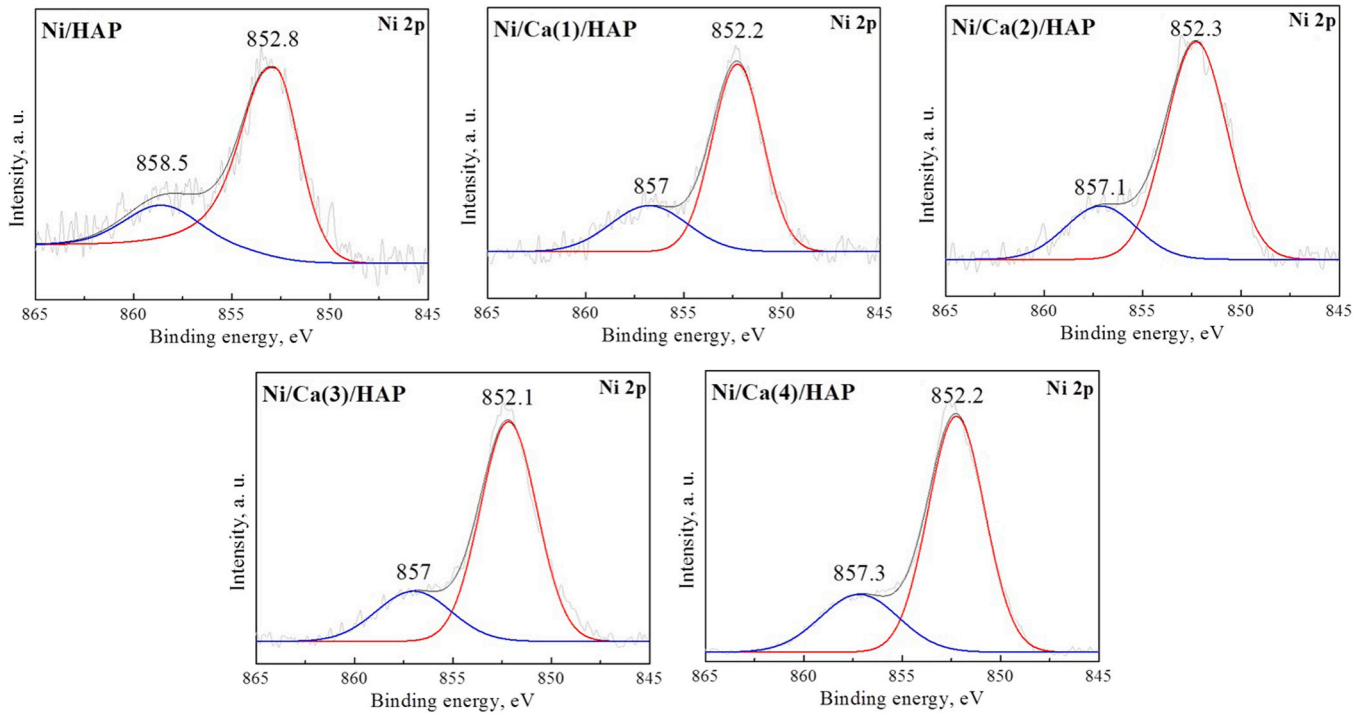

Fig. 4. XPS spectra (Ni $2p_{3/2}$ region) for the reduced Ni/Ca(x)/HAP samples.

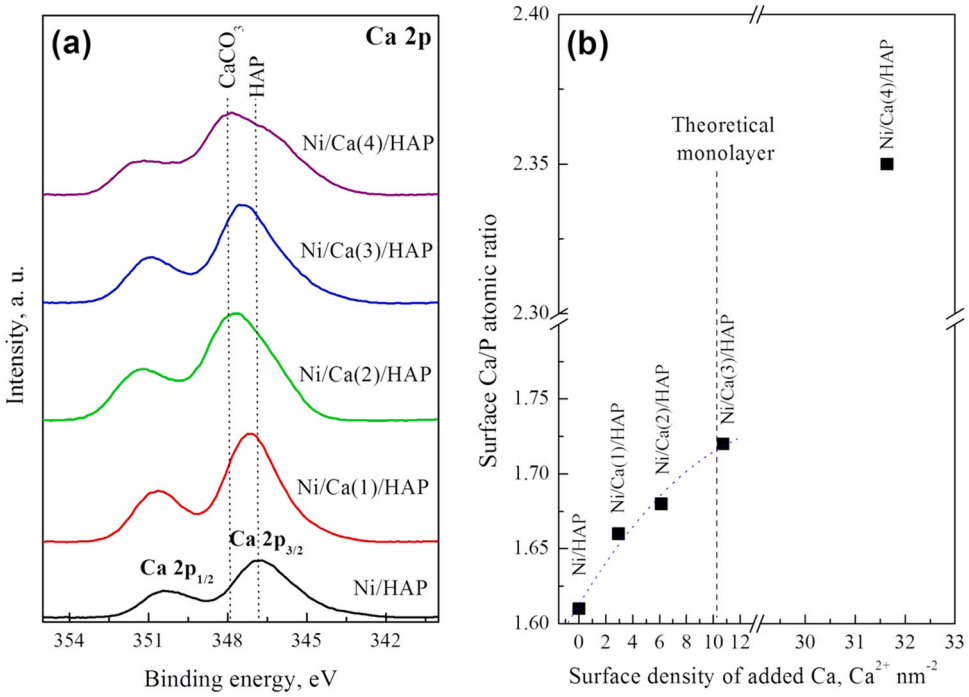

Fig. 5. (a) XPS spectra recorded in Ca 2p region of the reduced Ni/Ca(x)/HAP catalysts. (b) dependence of surface Ca/P atomic ratio (determined by XPS) on the surface density of added Ca.

Table 2
XPS data for the reduced Ni/Ca(x)/HAP samples.

Sample	Ni $2p_{3/2}$, eV	O 1 s, eV	Ca $2p_{3/2}$, eV	P 2p, eV	Ca/P	Ni/P	O/P	C/P (O-C═O)
Ni/HAP	852.8	531.0	346.7	133.2	1.61	0.04	3.7	0.03
Ni/Ca (1)/ HAP	852.2	530.9	347.1	133.3	1.66	0.06	3.7	0.05
Ni/Ca (2)/ HAP	852.3	531.7	347.6	133.9	1.68	0.08	3.7	0.07
Ni/Ca (3)/ HAP	852.1	531.3	347.4	133.2	1.72	0.14	3.7	0.08
Ni/Ca (4)/ HAP	852.2	531.7	347.9	133.9	2.35	0.45	4.5	0.15

local environment of surface Ca^{2+} ions, since a systematic shift towards higher BE values can be observed (from 346.7, for Ni/HAP, to 347.9 eV, for Ni/Ca(4)/HAP). In agreement with a number of earlier studies, this evolution indicates a progressive structural and chemical changes of surface Ca species, from CaO (347.2 eV [37]) to $CaCO_3$ species (347.7 eV [38]). The appearance of these Ca phases actually approves the main presence of surface species which do not integrate the HAP structure. On the other hand, data from Table 2 reveal that the estimated surface Ca/P atomic ratio clearly increases with the progressive addition of Ca; in accordance with XRD and HAADF data, this confirms once again that its deposition is uniform and no segregation of resulting species can be observed. Likewise, as it can be deduced from Fig. 5b, even working with a surface density of added Ca three times larger than that required for a deposition of a theoretical monolayer, there is no apparent segregation of its resulting phases. Instead, a volcano-type curve would be obtained. Fig. S4 displays the C 1 s spectra for all reduced samples. As it can be deduced from their analysis, the samples exhibit two typical peaks at 284.6 and 289.3 ± 0.7 eV, assigned to C-C/C-H and O-C═O species, respectively [39]. Interestingly, the contribution of the latter systematically increases with the Ca content (Table 2), confirming an enrichment of the catalyst near surface with $CaCO_3$ species most likely retained in the bulk of a ticker layer.

3.1.5. *Reducibility of the catalysts*

The reducibility of the as-prepared Ni/Ca(x)/HAP catalysts has been investigated by H_2-TPR techniques. The corresponding results are shown in Fig. 6. The reduction profile of Ni/HAP shows an intense peak at relatively low temperatures (345 °C), assigned to surface NiO species,

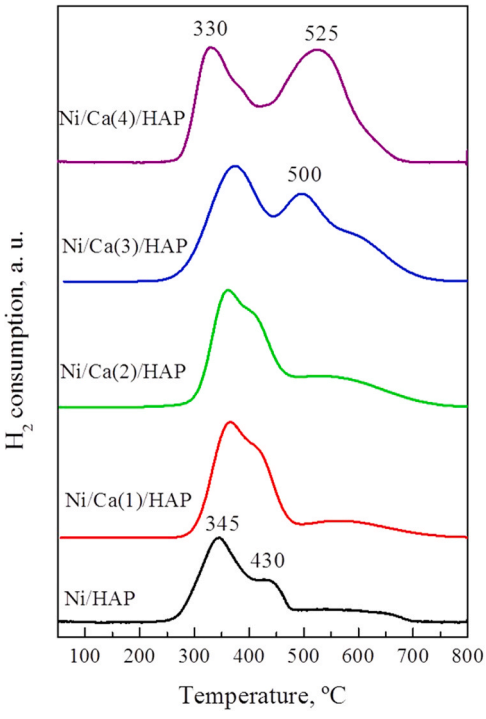

Fig. 6. H_2-TPR diagrams for Ni/Ca(x)/HAP catalysts.

and a shoulder around 430 °C, due to NiO strongly interacting with the support [8,29]. The addition of 1 wt% Ca slightly shifts the peaks towards higher temperatures, suggesting an increase in the strength of metal-support interactions. At a higher Ca loadings (≥ 2 wt%), the reduction process presents a complex profile with an important contribution of additional intense peaks at high temperatures (> 500 °C). Moreover, upon integration of the whole reduction profile, one can observe that the amounts of consumed H_2 systematically increase with Ca loading (Table 3). Especially, over the samples with high Ca loadings (> 1 wt%) the H_2 amounts are larger than those corresponding to a stoichiometric NiO phase. In agreement with XPS data, the observed trend can rather be explained by a thermal decomposition of surface carbonates. In order to evaluate this possibility the Ni/Ca(4)/HAP sample has further been subjected to a TPR-MS study, where the evolutions of the signals corresponding to CO_2, CO, CH_4 and H_2 with the temperature increase have been recorded. Indeed, according to Fig. S5, the reduction profile evidences the contribution of CH_4, CO_2 and CO signals at high temperatures (> 500 °C), resulting from the decomposition and/or reactivity of surface carbonate.

3.1.6. Surface basicity and reactivity studies

The impact of Ca addition on the surface basicity of reduced Ni/Ca (x)/HAP catalysts has been investigated by using CO_2-TPD techniques. The recorded diagrams and the corresponding quantitative data are shown in Fig. 7 and Table 3, respectively. The profile of HAP bare support consists of two CO_2 desorption regions. The first one (T < 500 °C) generally corresponds to weakly adsorbed CO_2, while the second domain (T > 500 °C) is assigned to strong adsorption sites [8]. The dispersion of nickel onto the HAP surface significantly increases the amounts of the adsorbed CO_2., from 80.3 $\mu mol_{CO2}\ g^{-1}$, for HAP, to 123.5 $\mu mol_{CO2}\ g^{-1}$, for NiHAP. It seems that the dispersion of Ni generates additional basic sites with different nature, most probably located at the Ni-HAP interface. According to the data from Fig. 7 and Table 3, this additional fraction mainly consists of weak basic sites. The addition of 1 wt% Ca dramatically increases the density of CO_2 adsorption sites (216.1 $\mu mol_{CO2}\ g^{-1}$), becoming almost double than that of the monometallic catalyst. Likewise, this significantly increases the contribution of the strong basic sites (from 34.3%, for Ni/HAP, to 57.9%, for Ni/Ca (1)/HAP). This effect seems to be more pronounced with the progressive addition of Ca, since on the sample with the highest Ca loading (4 wt%) the contribution of the highly stable basic sites reaches 97.5%. It should be noted that, our XPS and TPR data showed a similar trend, suggesting that this sample bears a large fraction of strongly adsorbed carbonates, probably forming $CaCO_3$ species.

The TPSR studies have been performed to assess the reactivity of the surface basic sites (Fig. 8). Fig. 8a displays the CH_4 formation diagrams for all Ni/Ca(x)/HAP samples. The monometallic catalyst (Ni/HAP) exhibits a main CH_4 production peak centered at 275 °C. The addition of 1 wt% Ca, however, leads to a broader production profile, peaked at 230

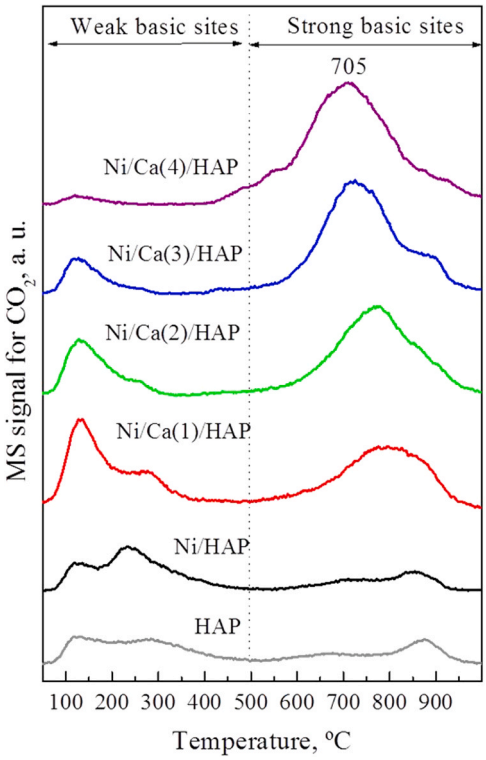

Fig. 7. CO_2-TPD diagrams for the reduced Ni/Ca(x)/HAP catalysts.

and 300 °C, indicating the occurrence of at least two distinct active sites. The presence of these two features can be associated with the existence of a fraction of Ni active centers exposed on the HAP surface and another fraction interacting, intimately, with surface Ca species, respectively. At higher Ca loadings (≥ 2 wt%) the CH_4 production domain shifts towards higher temperatures giving rise to much broader and intense peaks. In line with the XPS data, this evolution can be linked to the occurrence of different types of surface calcium-containing forms, ought to coexist in the Ca-enriched samples. Among them, a form accounting for strong CO_2 adsorption sites, most likely corresponds to bulk $CaCO_3$ weakly interacting with the HAP, which can be unequivocally identified on the Ni/Ca(4)/HAP sample giving rise to a peak centered at 530 °C. Furthermore, as deduced from Table 3, the progressive addition of Ca increases the density of produced CH_4 to reach a value close to 242.7 $\mu mol_{CH4}\ g^{-1}$ for the Ni/Ca(4)/HAP sample. In parallel, according to Fig. 8b, except for Ni/Ca(4)/HAP sample, the CO_2 desorption process, corresponding to unstable and inactive basic sites, mainly occurs at relatively low temperatures (T < 300 °C) and their density decreases with Ca loadings. By contrast, the fraction of thermally stable and inactive sites (T > 500 °C)

Table 3
H2-TPR, CO2-TPD, TPSR and CO2 methanation activity data for the reduced Ni/Ca(x)/HAP samples.

Sample	H_2-TPR		CO_2-TPD			TPSR	CO_2 methanation	
	Reducibility, $mmol_{H2}\ g^{-1}$	H_2/Ni [a]	Total basicity, $\mu mol_{CO2}\ g^{-1}$	Weak basic sites, % [b]	Strong basic sites, % [b]	Produced CH_4, $\mu mol_{CH4}\ g^{-1}$ [c]	r, $\mu mol_{CO2}\ g^{-1}\ s^{-1}$ (300 °C) [d]	E_a, kJ mol^{-1} (260–330 °C) [e]
HAP	-	-	80.3	56.7	43.3	-	-	-
Ni/HAP	0.57	0.82	123.5	65.7	34.3	40.4	5.6	73.8
Ni/Ca(1)/HAP	1	1.39	216.1	42.1	57.9	150.1	13	92.4
Ni/Ca(2)/HAP	1.22	1.25	210.3	26.1	73.9	201.8	35	93.3
Ni/Ca(3)/HAP	1.61	1.26	226.3	23.1	76.9	222.1	18	102
Ni/Ca(4)/HAP	1.77	1.39	238.5	2.5	97.5	242.7	3.5	94.8

(a) Calculated by integration of the peaks occurring at low temperatures (< 500 °C).
(b) Relative contribution of basic sites.
(c) Density of active sites involved in the methanation, determined by integration of CH_4 production peaks.
(d) CO_2 methanation reaction rate determined under differential reactor conditions.
(e) Activation energy.

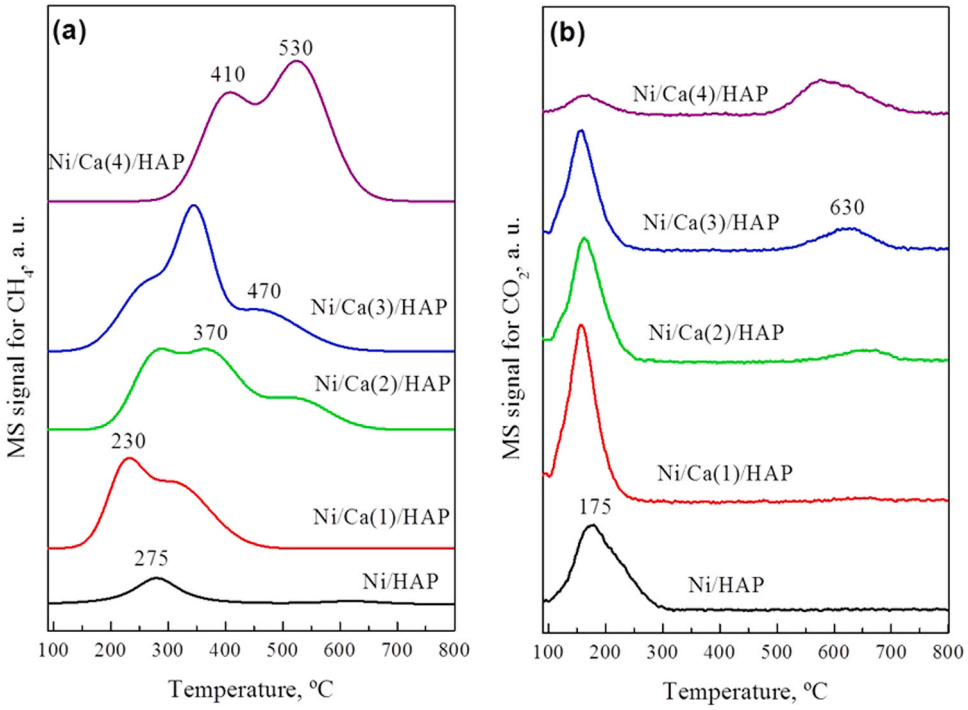

Fig. 8. TPSR diagrams for the reduced Ni/Ca(x)/HAP catalysts corresponding to (a) CH_4 and (b) CO_2 recorded signals.

systematically increases with Ca loading. (Table 4).

3.2. Catalytic performance

3.2.1. CCU-methanation performance over Ni/Ca(x)/HAP catalysts

Figs. 9a, 9b and 9c display the light-off curves of CO_2 conversion and selectivity towards CH_4 and CO production, respectively, during the CO_2 methanation reaction. It should be noted that the Ni/Ca(x)/HAP catalysts were previously reduced in a 20% H_2/He flow at 500 °C, for 1 h. As it can be deduced from Fig. 9a, all tested samples reach their maximum conversion, corresponding to the thermodynamic equilibrium (TE), at relatively low temperatures ($T_{max} \leq 500$ °C). With the reactor filled up with the unpromoted sample (Ni/HAP) the activity starts around 250 °C and increases with the reaction temperature to approach a value close to 50% at 375 °C, before reaching a maximum of 72% at 450 ºC and that of TE (70%) at 500 °C. The positive effect of Ca addition is already evidenced over the Ni/Ca(1)/HAP sample, since T_{50} and T_{max} temperatures of the monometallic sample shift to lower values (348 °C and 430 °C, respectively). This promoting effect is more pronounced with the addition of 2 wt% Ca, achieving the best catalytic performance among all tested samples ($T_{50} = 325$ °C and $T_{max} = 400$ °C). Further addition of Ca, however, decreases gradually the overall activity, where Ni/Ca(4)/HAP results even less active than the un-promoted sample. Accordingly, the activity of the investigated catalysts follows this general trend: Ni/Ca(2)/HAP > Ni/Ca(3)/HAP > Ni/Ca(1)/HAP > Ni/HAP > Ni/Ca(4)/HAP. Furthermore, according to Fig. 9b, the most active catalysts (Ni/Ca(2)/HAP and Ni/Ca(3)/HAP) prove to be more selective towards CH_4 production (S_{CH4}) at low temperatures (≤ 300 °C); whilst at higher temperatures all samples exhibit a comparable S_{CH4} values, becoming close to each other (> 92%). Note that the formation of relatively small amounts of CO (Fig. 9c) can be associated with the moderate acidity of the investigated support, which does not favor the reverse water-gas shift (RWGS) reaction [8].

Fig. 10a displays the dependence of turnover frequency (TOF), estimated according to differential reactor conditions and normalized by surface metallic Ni, on the amounts of Ca added. Interestingly, the

Table 4
Comparison of the performance of Ni/Ca(x)/HAP catalysts with catalyst formulations from the literature.

Catalyst	Ni, wt%	Feed gas composition: CO_2/H_2/He	WHSV, $cm^3\ h^{-1}\ g^{-1}$	T_{50}, ºC	T_{max}, ºC [(a)]	Ref.
Ni/HAP	3.3	1/4/1.25	30,000	375	450	This work
Ni/Ca(1)/HAP				348	450	
Ni/Ca(2)/HAP				325	425	
Ni/Ca(3)/HAP				338	450	
Ni/Ca(4)/HAP				400	500	
Ni/La(1)/HAP	3.2	1/4/1.25	30,000	368	450	[8]
Ni/La(3.7)/HAP				327	400	
Ni/La(6.6)/HAP				318	400	
Ni/Al_2O_3	20	1/5/1.5	30,000	318	475	[40]
Ni/CeO_2	5	1/4/1.25	30,000	357	500	[16]
$Ni/Ce_{0.85}Zr_{0.15}O_2$				337	500	
Ni/Pr-Ce	10	1/4/5	25,000	340	n.d.	[56]
$Ni/37La_2O_3/Al_2O_3$	13.6	1/5/10.7	54,420	330	450	[17]
$10\%LaNiO_3/CeO_2$	2.8	1/4/1.25	30,000	312	500	[57]
Ca-modified Ni-Al	10	1/4/0	15,000	275	> 450 ºC	[58]

Temperature corresponding to the thermodynamic equilibrium.

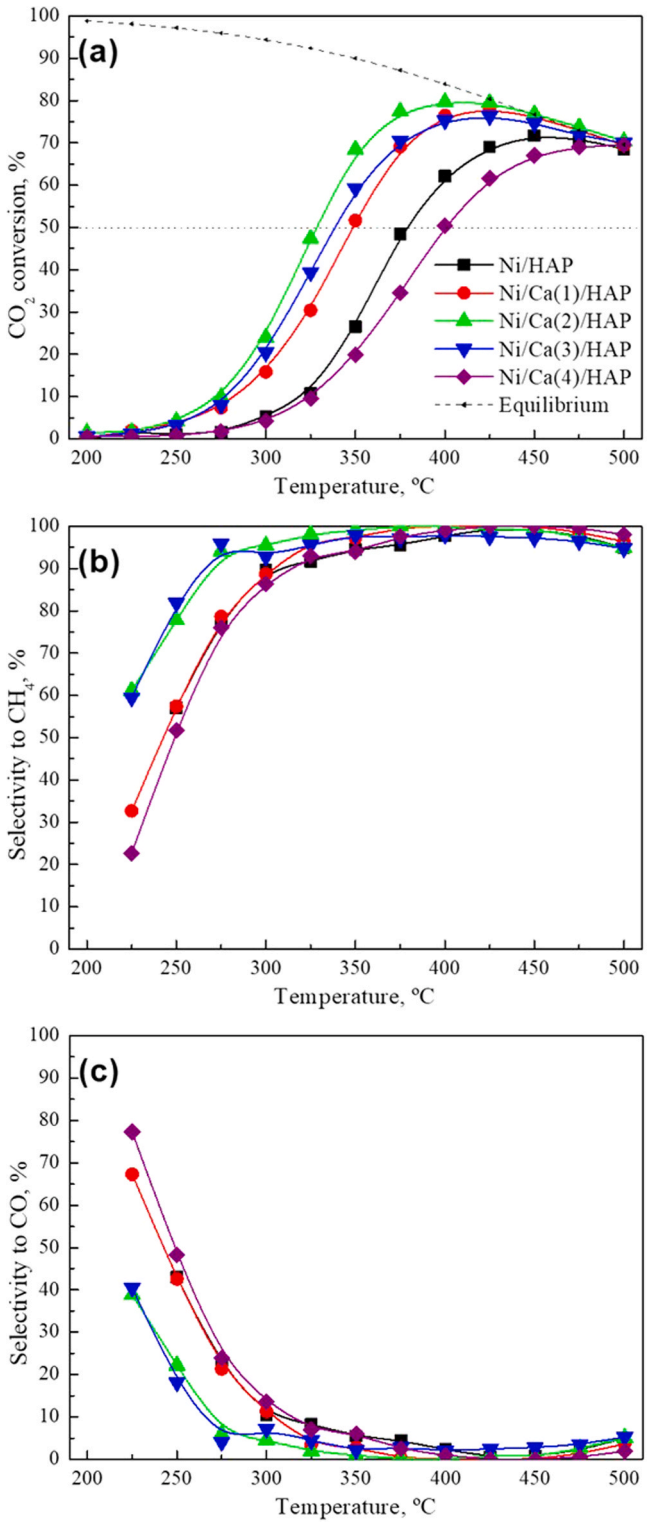

Fig. 9. Catalytic activity of the Ni/Ca(x)/HAP catalysts in the CO_2 methanation reaction. (a) CO_2 conversion, (b) selectivity to CH_4 and (c) selectivity to CO.

general trend consists on a volcano-type curve, evidencing once again a subtle superiority of the sample with 2 wt% Ca added (0.49 s^{-1}). This suggests that the latter probably comprises the most efficient Ni active species. It should be outlined that no direct correlation between the activity and Ni particle sizes can be deduced from the analysis of the data for the whole series of the assayed samples. For instance, Ni/Ca(1)/HAP (0.26 s^{-1}) results almost nine times more active than Ni/Ca(4)/HAP (0.03 s^{-1}), despite the fact that the former comprises larger Ni particle sizes (13.8 nm vs. 6.1 nm). Thus, one can conclude that the activity is rather dependent on other parameters involving the surface distribution of the promoter as well as the nature of the resulting surface chemistry. Previous reports pointed out that the CO_2 methanation reaction occurs through a bi-functional mechanism, in accordance with which the activation of H_2 takes place on surface Ni sites, whereas CO_2 is activated on the basic sites spread on the support surface [43–50]. In this sense, it is plausible that the activity of the assayed catalysts is also sensitive to the distribution of the surface basic sites and the nature of their interactions with the active phase. Besides its effect on the number and the distribution of basic sites, our XRD data point out that Ca addition induces the occurrence of defective metallic Ni crystallites, most likely located at Ni-Ca interfaces. According to the literature data, the presence of these surface defects at the metal-support interface provides highly active sites, essential for the CO_2 methanation [8,49,50]. In their study on the activity of ceria-based catalysts, Cárdenas-Arenas et al. [49] found that H_2 dissociation occurred on surface metallic Ni whilst the activation of CO_2 took place on the NiO-CeO_2 interface. When optimized an adequate relative contribution of each active species could affect positively on the catalytic performance. In this sense, though Ni/Ca(4)/HAP sample contains the largest density of Ni lattice defects, it shows the worst catalytic performance. This result can be associated with the poorest textural properties as well as the distribution of added Ca species. According to the XPS and TPD studies, over this sample surface Ca species are mostly deposited forming a thick layer, which probably weakens the interaction Ni-HAP and limits the occurrence of an advantageous synergistic effect of HAP support with Ni active phases. Moreover, Ni/Ca(4)/HAP bears the largest fraction of thermally stable basic sites (97%), most likely inactive and strongly retain CO_2 molecules, which actually limits their effective participation.

Activation energy (E_a) values obtained from the slope of the Arrhenius plots (Fig. 10b) have been calculated using differential reactor conditions (Table 3, last column). The monometallic sample presents a relatively low Ea (73.8 kJ mol^{-1}). However, irrespective of the amounts of Ca added, this value is significantly higher, becoming ranging between 92.4 and 102 kJ mol^{-1}, in agreement with those found in earlier studies [8,40–42]. The relatively lower E_a value observed over the unpromoted sample would imply differences in the mechanism pathway compared with the Ca-modified samples [8,15,17,46].

The stability experiment performed over the optimal Ni/Ca(2)/HAP sample (at 350 °C) reveals its robust performance (Fig. 11). The assayed catalyst shows an initial activity around 72%. After a smooth deactivation period of 8 h, a good stability can be observed, for 90 h TOS, maintaining CO_2 conversion close to 69% and a high selectivity to CH_4 formation (94%). According to HAADF microscopy data, reported in Fig. 12, the observed small deactivation is consistent with a slight growth of Ni particles, which show an increase in their average size from 9.4 to 10 nm (Fig. 12b and e, respectively). By contrast, BET and XRD analyses of the spent sample (not displayed) show that no significant differences can be observed, regarding its textural and structural properties, with respect to the freshly reduced sample.

3.2.2. *ICCU-methanation performance over Ni/Ca(x)/HAP DFMs*

The Ni/Ca(x)/HAP samples have also been assayed as DFMs under ICCU-methanation conditions. For this purpose, their performance during cycles of CO_2 storage followed by methanation in H_2 stream was evaluated. To figure out the details of these studies, we report in Fig. S6 the profiles of recorded CO_2, CO, H_2O and CH_4 signals, during a cycle of CO_2 capture and methanation over the Ni/Ca(3)/HAP DFM sample.

Fig. 13 (a-c) displays the evolution of the density of active CO_2 stored and produced CH_4 and CO with temperature, respectively, estimated during CO_2 adsorption and methanation period. It can be observed that irrespective of the amounts of Ca added, this significantly increases the density of stored CO_2 as well as the produced CH_4 and CO. At 400 °C, for

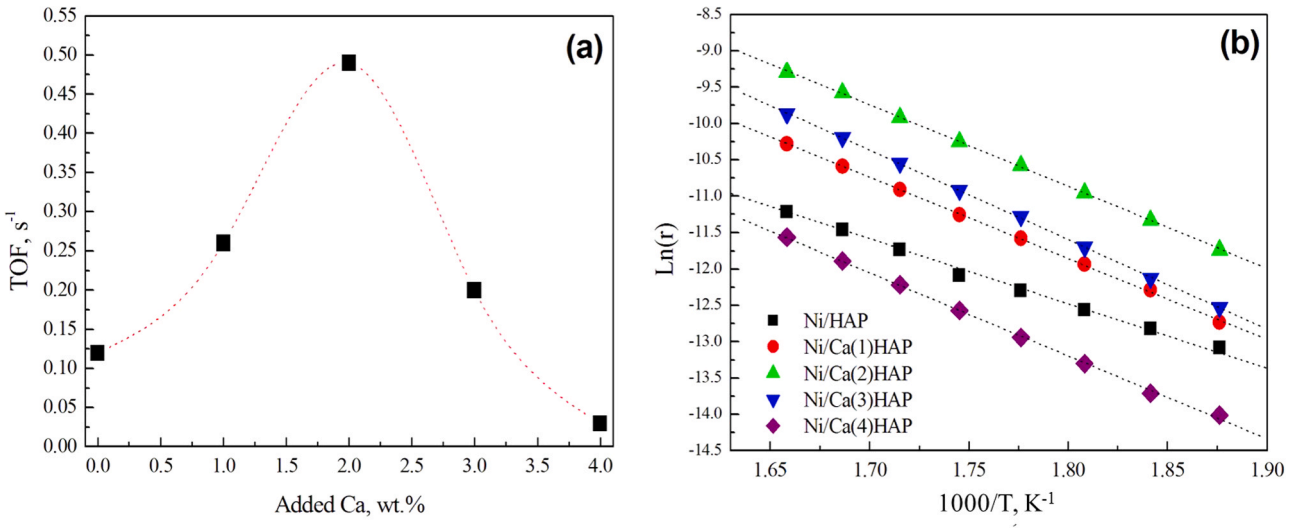

Fig. 10. (a) Dependence of TOF on Ca added loading and (b) Arrhenius plots for the Ni/Ca(x)/HAP catalysts.

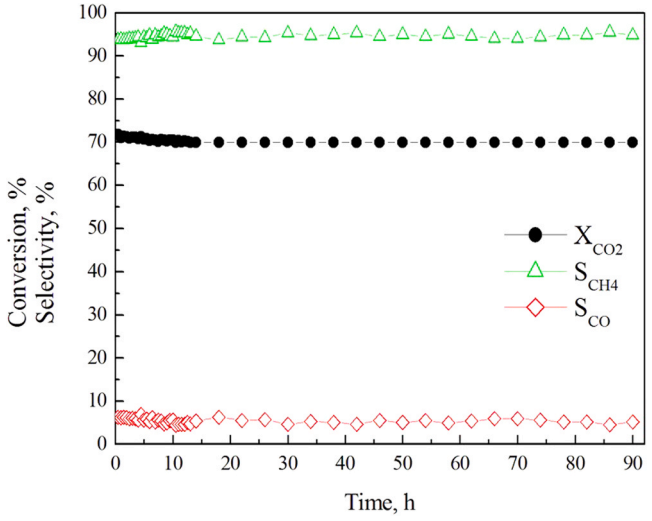

Fig. 11. Catalytic stability of the Ni/Ca(2)/HAP sample in the methanation reaction, at 350 ºC, in 16% CO_2 and 64% H_2, balanced in He (WHSV = 30,000 $cm^3\ g^{-1}\ h^{-1}$).

instance, the density of stored CO_2 estimated over the Ni/Ca(3)/HAP DFM (157.5 $\mu mol_{CO2}\ g^{-1}$) is about 4.5 times larger than that of the unpromoted sample (33.7 $\mu mol_{CO2}\ g^{-1}$). To the same extent, the former proves to be the most efficient DFM to convert the adsorbed CO_2 to CH_4, during the hydrogenation period, reaching a CH_4 density close to 155 $\mu mol_{CH4}\ g^{-1}$ at 400 °C. In parallel, small amounts of CO can be observed (3.1 $\mu mol_{CO}\ g^{-1}$). Interestingly, the performance of Ni/Ca(3)/HAP DFM sample clearly outperforms that reported over a 15%Ni/15%CaO/Al_2O_3 DFM tested under similar conditions [51]. On the latter, although it bore larger surface area (98 $m^2\ g^{-1}$) and both higher Ni and Ca loadings (15% and 10.7%, respectively) the measured methane production did not exceed 125 $\mu mol_{CH4}\ g^{-1}$ at 400 °C. Another comparison of the performance of our optimized sample with that reported by Jo et al. [52] reveals that the former represents an advantageous alternative as catalyst-sorbent for the ICCU-methanation process, since the application of their 9.3%Ni/CaO DFM did not display any methanation activity at 400 ºC.

As already outlined, the XRD, XPS and HAADF data clearly evidence that Ca is homogeneously dispersed on the HAP surface. Considering that the surface density of calcium in the Ni/Ca(3)/HAP DFM is close to the theoretical monolayer for Ca supported on HAP, we may accordingly assume that the fraction of free HAP surface is relatively very small, and therefore, its contribution to the adsorption of CO_2 can reasonably be neglected. Instead, the typical cyclic carbonation/decarbonation process mainly occurs over the surface CaO sorbent following the reaction (7). If so, the experimental amounts of stored CO_2 referred to 1 g of CaO, measured for Ni/Ca(3)/HAP DFM, would be close to 4 $mmol_{CO2}\ g_{CaO}^{-1}$ at 400 ºC. This value actually represents 22.5% of the theoretical CO_2 sorption capacity reported for a stoichiometric CaO phase [30,52]; which suggests that 77.5% of supported CaO does not provide any active CO_2. Note that this distribution is consistent with that corresponding to the contribution of weak and strong basic sites (23.1% and 76.9%, respectively), according to the TPD-CO_2 data reported in Table 3; suggesting that, at 400 ºC, the sorption activity involves the weak basic sites only.

$$CaO + CO_2 \rightleftarrows CaCO_3 \quad \Delta H^0 = -178 kJ\ mol^{-1} \tag{7}$$

Fig. 14 compares the specific activity of the studied DFMs, at 360 ºC, referred to 1 m^2 of the BET surface area. It can be deduced that the positive effect of Ca addition on methane production exhibits an upper limit, at 3 wt% Ca, reaching a surface density of 2.6 $\mu mol_{CH4}\ m^{-2}$, after which it stays almost constant. This result points out that the activity towards methane production involves surface CaO species only and, probably, would depend on the distance between Ni active sites and CaO sorbent. In this sense, according to our characterization data, we assume that the Ni^0-CaO distance decreases with Ca addition up to a shorter and critical value; which would correspond to Ni/Ca(3)/HAP and Ni/Ca(4)/HAP DFMs, where CaO totally covers the HAP support surface. A similar observation was reported by Porta et al. [53] in their study on Ru-BaO/Al_2O_3 DFMs for cyclic CO_2 capture and methanation. In addition, it also seems that maximizing the synergistic effects of CaO and HAP support results in the improvement of ICCU-methanation performance [54]. Our results actually contrast with those reported by Sun al. [55] in their study on Ni/CeO_2-CaO DFMs, since they claimed that a better ICCU performance, in terms of CH_4 selectivity, could be achieved with a surface distribution exhibiting larger Ni^0-CaO distances. They associated the poor performance of the DFMs presenting shorter Ni^0-CaO distances with a loss in the number of active sites due to the formation of $CaCO_3$ covering Ni phase. To a lesser extent, however, the surface density of CO production seems to increase with added Ca content, where the Ni/Ca(4)/HAP sample presents the largest value (0.042 $\mu mol_{CO2}\ m^{-2}$). This trend is consistent with the observed increase in the strength of the basic sites (Table 3) as well as the improvement of the dispersion of Ni active sites (Fig. S7), which probably favor the

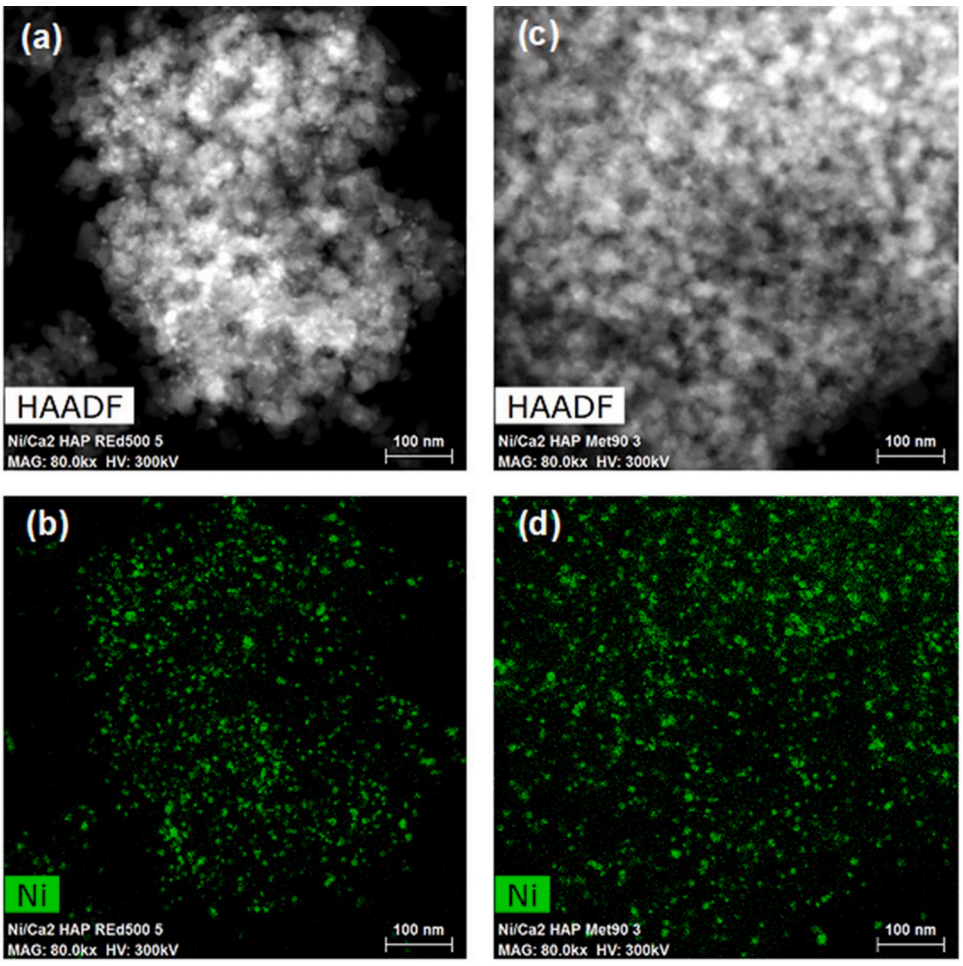

Fig. 12. HAADF images and the corresponding maps for Ni, given by X-EDS, for the Ni/Ca(2)/HAP sample: (a,b) freshly reduced sample and (c,d) sample submitted to the stability test at 350 °C for 90 h.

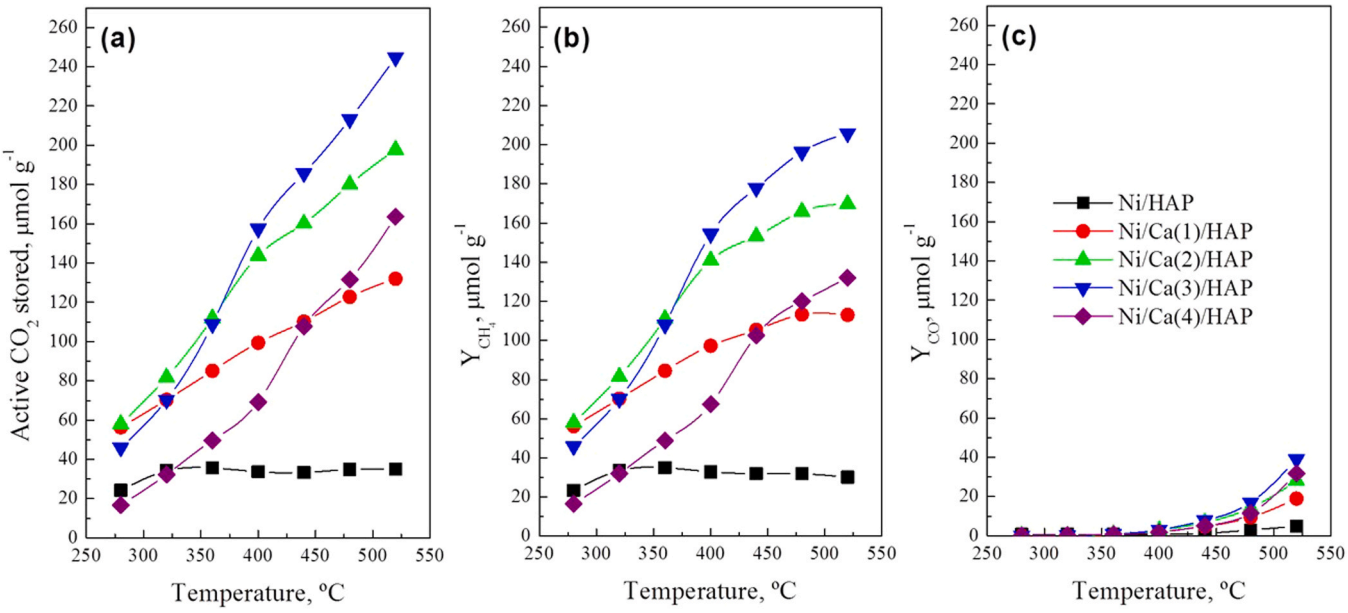

Fig. 13. ICCU-methanation performance of Ni/Ca(x)/HAP DFMs. Evolution of (a) active CO_2 stored and production of (b) CH_4 and (c) CO versus the temperature, under cycling CO_2 storage/reduction process conditions.

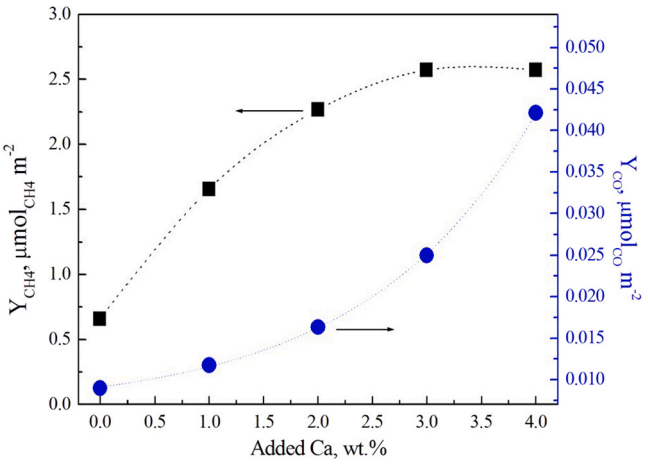

Fig. 14. Dependence of surface activity (in terms of produced CH_4 and CO surface density) in ICCU-methanation process on the amounts of added Ca.

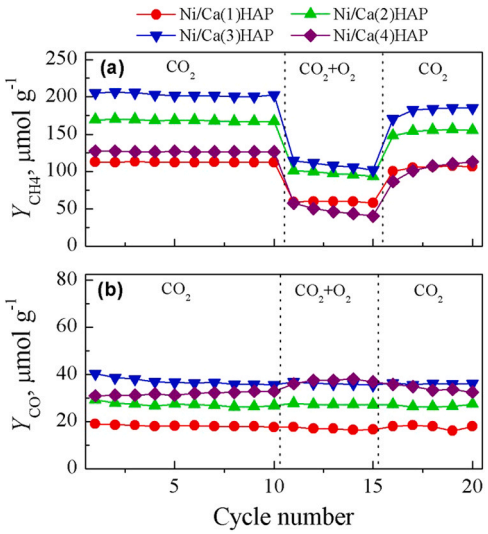

Fig. 15. Effect of O_2 addition on the ICCU-methanation performance of Ni/Ca (x)/HAP DFMs in cyclic tests of CO_2 adsorption and methanation, performed at 520 °C.

occurrence of the RWGS reaction. Phey Phey et al. [59] also associated the efficiency of their Cu/ZnO catalysts for RWGS reaction with the abundance of strong basic sites. Previous reports claimed that over some surface metallic sites a dissociative adsorption of CO_2 could take place to produce CO and O species [60–62]. The latter seem to spillover to strong basic sites and then react with H_2 to produce H_2O.

The capacity of Ni/Ca(x)/HAP DFMs to endure more severe conditions has been investigated at 520 °C for twenty consecutive CO_2 capture and direct methanation cycles, including five cycles under oxidative conditions as well, where 10% O_2 is added to the feed corresponding to the CO_2 capture period. According to Fig. 15, with reference to free oxygen conditions, over all tested DFMs the addition of O_2 markedly lowers the amount of produced CH_4. For instance, over the most efficient DFM (Ni/Ca(3)/HAP) methane production decreases from 210 to 105 µmol$_{CH4}$ g^{-1}, probably due to the oxidation of Ni active sites [8,63,64]. However, no significant change can be observed concerning the amounts of produced CO. Interestingly, once O_2 is removed during the CO_2 capture period, all samples tend to recover their initial activity, shown in absence of O_2, suggesting that the observed deactivation is rather a reversible process.

4. Conclusions

The viability of Ni supported on Ca-enriched HAP samples has been investigated for the intensification of CCU-methanation and ICCU-methanation decarbonization processes.

According to the characterization data, due to its affinity with HAP support, addition of Ca provides a suitable distribution of its surface species. For instance, even working with a surface density of added Ca (31.6 Ca^{2+} nm^{-2}), three times larger than that required for a deposition of a theoretical monolayer (10.3 Ca^{2+} nm^{-2}), there is no apparent segregation of phases. In addition, the progressive addition of calcium dramatically increases both the number and the strength of basic sites. Likewise, this markedly increases the Ni dispersion and the density of Ni lattice defects.

The addition of Ca amounts ranging between 1 and 3 wt% results in a dramatic improvement of the CCU-methanation activity and selectivity, when compared with the Ni/HAP reference sample. This promoting effect is more pronounced with the addition of 2 wt% Ca; achieving the best catalytic performance among all tested samples (TOF = 0.49 s^{-1}, T_{50} = 325 °C and T_{max} = 400 °C). Likewise, it shows a good stability in a long-term stability test at 375 °C for 90 h TOS. A compromise between the surface chemistry and the distribution of Ni active sites proves to be the key factor influencing the efficiency of the investigated materials. For instance, though it contains the smallest Ni NPs, the Ni/Ca(4)/HAP sample results less active due to the presence of the largest fraction of thermally stable basic sites (97%), most likely inactive and strongly retain CO_2 molecules, which actually limits their effective participation.

The Ni/Ca(x)/HAP samples have also been tested as DFMs in the ICCU-methanation process in the temperature range of 280–520 °C. In this case, the Ni/Ca(3)/HAP DFM with added Ca loading close to the theoretical monolayer exhibits the best performance. For instance, it proves to be the most efficient to convert the stored CO_2 to CH_4, during the reduction period, reaching a CH_4 density close to 155 µmol$_{CH4}$ g^{-1} at 400 °C. In parallel, small amounts of CO can be observed (3.1 µmol$_{CO}$ g^{-1}). It is supposed that the methanation activity involves CO_2 stored on surface CaO species only and it is most likely improved over DFMs exhibiting short Ni^0-CaO distances. Interestingly, the performance of our Ni/Ca(3)/HAP DFM sample clearly outperforms that reported over 15% Ni/15%CaO/Al_2O_3 and 9.3%Ni/CaO reference DFMs. We may conclude that the dispersion of Ca on HAP support, with loadings close to the theoretical monolayer, results in an interesting alternative to traditional basic DFMs.

CRediT authorship contribution statement

Zouhair Boukha: Conceptualization, Methodology, Investigation, Writing – original draft. **Alejandro Bermejo-López:** Investigation, Experimentation, Writing – original draft. **Unai De-La-Torre:** Visualization, Verification, Writing – review & editing. **Juan R. González-Velasco:** Conceptualization, Supervision, Writing – review & editing, Project administration, Funding acquisition.

Declaration of Competing Interest

The authors declare that they have no known competing financial interests or personal relationships that could have appeared to influence the work reported in this paper.

Data Availability

Data will be made available on request.

Acknowledgements

The authors are indebted to Spanish Science and Innovation Ministry (PID2019-105960RB-C21 MCIN/AEI /10.13039/501100011033) and

Project IT1509-2022 by the Basque Government for the financial support. The support from SGIker (UPV/EHU ERDF, EU) is also acknowledged.

Appendix A. Supporting information

Supplementary data associated with this article can be found in the online version at doi:10.1016/j.apcatb.2023.122989.

References

[1] G. Taylor, S. Vink, Managing the risks of missing international climate targets, Clim. Risk Manag. 34 (2021), 100379.
[2] S. Sun, H. Sun, P.T. Williams, C. Wu, Recent advances in integrated CO_2 capture and utilization: a review, Sustain. Energy Fuels 5 (2021) 4546–4559.
[3] A.I. Tsiotsias, N.D. Charisiou, I.V. Yentekakis, M.A. Goula, The role of alkali and alkaline earth metals in the CO_2 methanation reaction and the combined capture and methanation of CO_2, Catalysts 10 (2020) 812.
[4] I.S. Omodolor, H.O. Otor, J.A. Andonegui, B.J. Allen, A.C. Alba-Rubio, Dual-function materials for CO_2 capture and conversion: a review, Ind. Eng. Chem. Res. 59 (2020) 17612–17631.
[5] P.M. Bravo, D.P. Debecker, Combining CO_2 capture and catalytic conversion to methane, Waste Dispos. Sustain. Energy 1 (2019) 53–65.
[6] S.B. Walker, D. van Lanen, U. Mukherjee, M. Fowler, Greenhouse gas emissions reductions from applications of power-to-gas in power generation, Sustain. Energ. Technol. Assess. 20 (2017) 25–32.
[7] D. Hidalgo, J.M. Martín-Marroquín, Power-to-methane, coupling CO_2 capture with fuel production: an overview, Renew. Sust. Energ. Rev. 132 (2020), 110057.
[8] Z. Boukha, A. Bermejo-López, B. Pereda-Ayo, J.A. González-Marcos, J.R. González-Velasco, Study on the promotional effect of lanthana addition on the performance of hydroxyapatite-supported Ni catalysts for the CO_2 methanation reaction, Appl. Catal. B-Environ. 314 (2022), 121500.
[9] Z. Lv, J. Ruan, W. Tu, X. Hu, D. He, X. Huang, C. Qin, Integrated CO_2 capture and In-Situ methanation by efficient dual functional Li_4SiO_4@Ni/CeO_2, Sep. Purif. Technol. 309 (2023), 123044.
[10] S. Cimino, R. Russo, L. Lisi, Insights into the cyclic CO_2 capture and catalytic methanation over highly performing Li-Ru/Al_2O_3 dual function materials, Chem. Eng. J. 428 (2022), 131275.
[11] Z. Liu, X. Gao, B. Liu, Q. Ma, T. Zhao, J. Zhang, Recent advances in thermal catalytic CO_2 methanation on hydrotalcite-derived catalysts, Fuel 321 (2022), 124115.
[12] J. Chen, Y. Xu, P. Liao, H. Wang, H. Zhou, Recent progress in integrated CO_2 capture and conversion process using dual function materials: a state-of-the-art review, Carbon Capture Sci. Technol. 4 (2022), 100052.
[13] S. Cimino, E.M. Cepollaro, L. Lisi, Ageing study of Li-Ru/Al_2O_3 dual function material during the integrated CO_2 capture and methanation with SO_2-containing flue gas, Carbon Capture, Sci. Technol. 6 (2023), 100096.
[14] T.A. Le, J. Kim, J.K. Kang, E.D. Park, CO and CO_2 methanation over M (MMn, Ce, Zr, Mg, K, Zn, or V)-promoted Ni/Al@Al_2O_3 catalysts, Catal. Today 348 (2020) 80–88.
[15] A. Quindimil, U. De-La-Torre, B. Pereda-Ayo, J.A. González-Marcos, J.R. González-Velasco, Ni catalysts with La as promoter supported over Y- and BETA- zeolites for CO_2 methanation, Appl. Catal. B Environ. 238 (2018) 393–403.
[16] I. Iglesias, A. Quindimil, F. Mariño, U. De-La-Torre, J.R. González-Velasco, Zr promotion effect in CO_2 methanation over ceria supported nickel catalysts, Int. J. Hydrog. Energ. 44 (2019) 1710–1719.
[17] G. Garbarino, C. Wang, T. Cavattoni, E. Finocchio, P. Riani, M. Flytzani-Stephanopoulos, G. Busca, A study of Ni/La-Al_2O_3 catalysts: a competitive system for CO_2 methanation, Appl. Catal. B-Environ. 248 (2019) 286–297.
[18] M. Guo, G. Lu, The difference of roles of alkaline-earth metal oxides on silica-supported nickel catalysts for CO_2 methanation, RSC Adv. 4 (2014) 58171–58177.
[19] W. Yang, Y. Feng, W. Chu, Promotion effect of CaO modification on mesoporous Al_2O_3-supported Ni catalysts for CO_2 methanation, Int. J. Chem. Eng. 2016 (2016) 1–7.
[20] O.E. Everett, P.C. Zonetti, O.C. Alves, R.R. de Avillez, L.G. Appel, The role of oxygen vacancies in the CO_2 methanation employing Ni/ZrO_2 doped with Ca, Int. J. Hydrog. Energ. 45 (2020) 6352–6359.
[21] K.H. Chai, L.K. Leong, D.S.- Wong, D.- Tsai, S. Sethupathi, Effect of CO_2 adsorbents on the Ni-based dual-function materials for CO_2 capturing and in situ methanation, J. Chin. Chem. Soc. 67 (2020) 998–1008.
[22] Z. Boukha, J.L. Ayastuy, M. Cortés-Reyes, L.J. Alemany, M.A. Gutiérrez-Ortiz, J. R. González-Velasco, Catalytic properties of cobalt-promoted Pd/HAP catalyst for CO-cleanup of H_2-rich stream, Int. J. Hydrog. Energ. 43 (2018) 16949–16958.
[23] Z. Boukha, J.L. Ayastuy, J.R. González-Velasco, M.A. Gutiérrez-Ortiz, Water-gas shift reaction over a novel Cu-ZnO/HAP formulation: Enhanced catalytic performance in mobile fuel cell applications, Appl. Catal. A-Gen. 566 (2018) 1–14.
[24] Z. Boukha, A. Choya, M. Cortés-Reyes, B. de Rivas, L.J. Alemany, J.R. González-Velasco, J.I. Gutiérrez-Ortiz, R. López-Fonseca, Influence of the calcination temperature on the activity of hydroxyapatite-supported palladium catalyst in the methane oxidation reaction, Appl. Catal. B-Environ. 277 (2020), 119280.
[25] Z. Boukha, J.R. González-Velasco, M.A. Gutiérrez-Ortiz, Viability of Au/La_2O_3/HAP catalysts for the CO preferential oxidation reaction under reformate gas conditions, Appl. Catal. B-Environ. 312 (2022), 121384.
[26] Z. Boukha, J.R. González-Velasco, M.A. Gutiérrez-Ortiz, Exceptional performance of gold supported on fluoridated hydroxyapatite catalysts in CO-cleanup of H_2-rich stream: High activity and resistance under PEMFC operation conditions, Appl. Catal. B Environ. 292 (2021), 120142.
[27] Z. Boukha, J.R. González-Velasco, M.A. Gutiérrez-Ortiz, Platinum supported on lanthana-modified hydroxyapatite samples for realistic WGS conditions: On the nature of the active species, kinetic aspects and the resistance to shut-down/start-up cycles, Appl. Catal. B-Environ. 270 (2020), 118851.
[28] Z. Boukha, B. Rivas, J.R. González-Velasco, J.I. Gutiérrez-Ortiz, R. López-Fonseca, Comparative study of the efficiency of different noble metals supported on hydroxyapatite in the catalytic lean methane oxidation under realistic conditions, Materials 14 (2021) 3612.
[29] Z. Boukha, M.P. Yeste, M.Á. Cauqui, J.R. González-Velasco, Influence of Ca/P ratio on the catalytic performance of Ni/hydroxyapatite samples in dry reforming of methane, Appl. Catal. A-Gen. 580 (2019) 34–45.
[30] H.J. Yoon, K.B. Lee, Introduction of chemically bonded zirconium oxide in CaO-based high-temperature CO_2 sorbents for enhanced cyclic sorption, Chem. Eng. J. 355 (2019) 850–857.
[31] H. Wang, W. Mo, X. He, X. Fan, F. Ma, S. Liu, D. Tax, Effect of Ca promoter on the structure, performance, and carbon deposition of Ni-Al_2O_3 catalyst for CO_2-CH_4 reforming, ACS Omega 5 (2020) 28955–28964.
[32] J.I. Langford, A.J.C. Wilson, Scherrer after sixty years: a survey and some new results in the determination of crystallite size, J. Appl. Crystallogr 11 (1978) 102–113.
[33] E.R. Shaaban, M. El-Hagary, E.S. Moustafa, H.S. Hassan, Y.A.M. Ismail, M. Emam-Ismail, A.S. Ali, Structural, linear and nonlinear optical properties of co-doped ZnO thin films, Appl. Phys. A Mater. 122 (2016) 1–10.
[34] S. Sun, C. Zhang, S. Guan, S. Xu, P.T. Williams, C. Wu, Ni/support-CaO bifunctional combined materials for integrated CO_2 capture and reverse water-gas shift reaction: Influence of different supports, Sep. Purif. Technol. 298 (2022), 121604.
[35] Y. Tanizawa, H. Tsuchikane, K. Sawamura, T. Suzuki, Reaction characteristics of hydroxyapatite with F^- and PO_3F^{2-} ions. Chemical states of fluorine in hydroxyapatite, J. Chem. Soc. Faraday T 87 (1991) 2235–2240.
[36] M.A. Stranick, M.J. Root, Influence of strontium on monofluorophosphate uptake by hydroxyapatite XPS characterization of the hydroxyapatite surface, Colloid Surf. 55 (1991) 137–147.
[37] P. Selvam, B. Viswanathan, V. Srinivasan, XPS studies of the surface properties of CaNi5, J. Electron. Spectrosc. 49 (1989) 203–211.
[38] S.L. Stipp, M.F. Hochella, Structure and bonding environments at the calcite surface as observed with X-ray photoelectron spectroscopy (XPS) and low energy electron diffraction (LEED), Geochim. Cosmochim. Acta 55 (1991) 1723–1736.
[39] B. Sivaranjini, R. Mangaiyarkarasi, V. Ganesh, S. Umadevi, Vertical alignment of liquid crystals over a functionalized flexible substrate, Sci. Rep. 8 (2018) 8891.
[40] A. Quindimil, U. De-La-Torre, B. Pereda-Ayo, A. Davó-Quiñonero, E. Bailón-García, D. Lozano-Castelló, J.A. González-Marcos, A. Bueno-López, J.R. González-Velasco, Effect of metal loading on the CO_2 methanation: a comparison between alumina supported Ni and Ru catalysts, Catal. Today 356 (2020) 419–432.
[41] C.V. Miguel, A. Mendes, L.M. Madeira, Intrinsic kinetics of CO_2 methanation over an industrial nickel-based catalyst, J. CO_2 Util. 25 (2018) 128–136.
[42] T. Van Herwijnen, H. Van Doesburg, W.A. De, Jong, Kinetics of the methanation of CO and CO_2 on a nickel catalyst, J. Catal. 28 (1973) 391–402.
[43] S.T. Yang, J. Kim, W.S. Ahn, CO_2 adsorption over ion-exchanged zeolite beta with alkali and alkaline earth metal ions, Micro Mesopor. Mat. 135 (2010) 90–94.
[44] P. Hongmanorom, J. Ashok, G. Zhang, Z. Bian, M.H. Wai, Y. Zeng, S. Xi, A. Borgna, S. Kawi, Enhanced performance and selectivity of CO_2 methanation over phyllosilicate structure derived Ni-Mg/SBA-15 catalysts, Appl. Catal. B-Environ. 282 (2021), 119564.
[45] D. Wierzbicki, R. Debek, M. Motak, T. Grzybek, M.E. Gálvez, P. Da Costa, Novel Ni-La-hydrotalcite derived catalysts for CO_2 methanation, Catal. Commun. 83 (2016) 5–8.
[46] Q. Pan, J. Peng, T. Sun, S. Wang, S. Wang, Insight into the reaction route of CO_2 methanation: promotion effect of medium basic sites, Catal. Commun. 45 (2014) 74–78.
[47] P. Riani, I. Valsamakis, T. Cavattoni, V. Sanchez Escribano, G. Busca, G. Garbarino, Ni/SiO_2-Al_2O_3 catalysts for CO_2 methanation: effect of La_2O_3 addition, Appl. Catal. B-Environ. 284 (2021), 119697.
[48] T. Burger, P. Donaubauer, O. Hinrichsen, On the kinetics of the co-methanation of CO and CO_2 on a co-precipitated Ni-Al catalyst, Appl. Catal. B-Environ. 282 (2021), 119408.
[49] A. Cárdenas-Arenas, H.S. Cortés, E. Bailón-García, A. Davó-Quiñonero, D. Lozano-Castelló, A. Bueno-López, Active, selective and stable NiO-CeO_2 nanoparticles for CO_2 methanation, Fuel Process. Technol. 212 (2021), 106637.
[50] A. Cárdenas-Arenas, A. Quindimil, A. Davó-Quiñonero, E. Bailón-García, D. Lozano-Castelló, U. De-La-Torre, B. Pereda-Ayo, J.A. González-Marcos, J. R. González-Velasco, A. Bueno-López, Design of active sites in Ni/CeO_2 catalysts for the methanation of CO_2: tailoring the Ni-CeO_2 contact, Appl, Mater. Today 19 (2020), 100591.
[51] A. Bermejo-López, B. Pereda-Ayo, J.A. González-Marcos, J.R. González-Velasco, Ni loading effects on dual function materials for capture and in-situ conversion of CO_2 to CH_4 using CaO or Na_2CO_3, J. CO_2 Util. 34 (2019) 576–587.
[52] S.B. Jo, J.H. Woo, J.H. Lee, T.Y. Kim, H.I. Kang, S.C. Lee, J.C. Kim, A novel integrated CO_2 capture and direct methanation process using Ni/CaO catal-sorbents, Sustain. Energy Fuels 4 (2020) 4679–4687.
[53] A. Porta, C.G. Visconti, L. Castoldi, R. Matarrese, C. Jeong-Potter, R. Farrauto, L. Lietti, Ru-Ba synergistic effect in dual functioning materials for cyclic CO_2 capture and methanation, Appl. Catal. B-Environ. 283 (2021), 119654.

[54] C. Ping, B.-Q. Feng, Y.-L. Teng, H.-Q. Chen, S.-L. Liu, Y.-L. Tai, H.-N. Liu, B.-X. Dong, Acquiring an effective CaO-based CO_2 sorbent and achieving selective methanation of CO_2, RSC Adv. 10 (2020) 21509–21516.
[55] H. Sun, Y. Wang, S. Xu, A.I. Osman, G. Stenning, J. Han, S. Sun, D. Rooney, P. T. Williams, F. Wang, C. Wu, Understanding the interaction between active sites and sorbents during the integrated carbon capture and utilization process, Fuel 286 (2021), 119308.
[56] G.I. Siakavelas, N.D. Charisiou, S. AlKhoori, A.A. AlKhoori, V. Sebastian, S. J. Hinder, M.A. Baker, I.V. Yentekakis, K. Polychronopoulou, M.A. Goula, Highly selective and stable nickel catalysts supported on ceria promoted with Sm_2O_3, Pr_2O_3 and MgO for the CO_2 methanation reaction, Appl. Catal. B-Environ. 282 (2021), 119562.
[57] J.A. Onrubia-Calvo, B. Pereda-Ayo, J.A. González-Marcos, A. Bueno-López, J. R. González-Velasco, Design of CeO_2-supported $LaNiO_3$ perovskites as precursors of highly active catalysts for CO_2 methanation, Catal. Sci. Technol. 11 (2021) 6065–6079.
[58] L. Xu, H. Yang, M. Chen, F. Wang, D. Nie, L. Qi, X. Lian, H. Chen, M. Wu, CO_2 methanation over Ca doped ordered mesoporous Ni-Al composite oxide catalysts: The promoting effect of basic modifier, J. CO_2 Util. 21 (2017) 200–210.
[59] M.L. Phey Phey, T.A. Tuan Abdullah, U.F. Md Ali, M.Y. Mohamud, M. Ikram, W. Nabgan, Reverse water gas shift reaction over a Cu/ZnO catalyst supported on regenerated spent bleaching earth (RSBE) in a slurry reactor: the effect of the Cu/Zn ratio on the catalytic activity, RSC Adv. 13 (2023) 3039–3055.
[60] M. Pachecka, J.M. Sturm, C.J. Lee, F. Bijkerk, Adsorption and dissociation of CO_2 on Ru(0001), J. Phys. Chem. C 121 (2017) 6729–6735.
[61] D.L. Jurković, A. Pohar, V.D.B.C. Dasireddy, B. Likozar, Effect of copper-based catalyst support on reverse water-gas shift reaction (RWGS) activity for CO_2 reduction, Chem. Eng. Technol. 40 (2017) 973–980.
[62] K.- Ernst, C.T. Campbell, G. Moretti, Kinetics of the reverse water-gas shift reaction over Cu(110), J. Catal. 134 (1992) 66–74.
[63] F. Kosaka, Y. Liu, S.- Chen, T. Mochizuki, H. Takagi, A. Urakawa, K. Kuramoto, Enhanced activity of integrated CO_2 capture and reduction to CH_4 under pressurized conditions toward atmospheric CO_2 utilization, ACS Sustain. Chem. Eng. 9 (2021) 3452–3463.
[64] M.A. Arellano-Treviño, Z. He, M.C. Libby, R.J. Farrauto, Catalysts and adsorbents for CO_2 capture and conversion with dual function materials: Limitations of Ni-containing DFMs for flue gas, Appl. J. CO_2 Util. 31 (2019) 143–151.